The Journal of Experimental Biology 207, 4651-4662
Published by The Company of Biologists 2004
doi:10.1242/jeb.01321

Submaximal power output from the dorsolongitudinal flight muscles of the hawkmoth *Manduca sexta*

Michael S. Tu* and Thomas L. Daniel
Department of Biology, University of Washington, Seattle WA 98195-1800, USA
*Author for correspondence (e-mail: mstu@u.washington.edu)

Accepted 1 October 2004

Summary

To assess the extent to which the power output of a synchronous insect flight muscle is maximized during flight, we compared the maximum potential power output of the mesothoracic dorsolongitudinal (dl_1) muscles of *Manduca sexta* to their power output *in vivo*. Holding temperature and cycle frequency constant at 36°C and 25 Hz, respectively, we varied the phase of activation, mean length and strain amplitude. Under *in vivo* conditions measured in tethered flight, the dl_1 muscles generated only 40–67% of their maximum potential power output. Compared to the *in vivo* phase of activation, the phase that maximized power output was advanced by 12% of the cycle period, and the length that maximized power output was 10% longer than the *in vivo* operating length.

Key words: flight, muscle, work, power, *Manduca sexta*.

Introduction

Over the last two decades, work loop studies have provided new insights into the principles of design that underlie muscle performance. In particular, a growing number of studies have compared maximal power output under experimental conditions to realized power output *in vivo*. The diversity in performance revealed by such comparisons suggests that maximization of power output (Hill, 1950), may not be the dominant principle underlying the design of muscle systems used in locomotion. Muscles may indeed attain their maximal power output during escape responses (Lutz and Rome, 1996; Askew and Marsh, 2001; Askew et al., 2001; Franklin and Johnston, 1997; James and Johnston, 1998). During sustained locomotion, however, maximal power output may be rare (Syme and Shadwick, 2002). Some of the observed diversity in muscle performance may reflect differences in function such as power generation *vs* stability and control (Full et al., 1998; Ahn and Full, 2002; Tu and Dickinson, 1994). Variation in muscle performance may also reflect fundamental differences in the demands on muscles in terrestrial locomotion *vs.* swimming and flight.

During terrestrial locomotion, muscles function in weight support and braking (Full et al., 1998; Ahn and Full, 2002), mechanical energy transfer (Olson and Marsh, 1998), and elastic strain energy storage and recovery (Roberts et al., 1997; Biewener et al., 1998). These demands may place constraints on muscle design that conflict with maximal power generation. During swimming and flying, relaxation of these constraints may permit muscles to operate closer to the conditions of strain and activation that maximize power output. Support for this view comes from the recent demonstration of maximal power generation by the deep red trunk muscle of swimming skipjack tuna (Syme and Shadwick, 2002). The unique anatomical arrangement of the red muscle of skipjack tuna and other thunniform swimmers may be critical in allowing these muscles to function solely as a motor. This high level of performance, however, may be the exception rather than the rule during steady swimming in fish. For example, in carangiform swimmers, the trunk muscles do not achieve their maximum potential power output during sustained swimming (Rome et al., 1999; Swank and Rome, 2001; Josephson, 1997; Coughlin, 2000; Hammond et al., 1998).

We currently lack the direct comparisons between realized and optimized power output necessary to assess the extent to which power output is maximized during flight. During take-off, the power generated by the pectoralis muscle of quail (Askew et al., 2001) is substantially higher than that reported for cockatiels during steady flight (Hedrick et al., 2003). While such extraordinary high levels of power generation may be an adaptation of ground-dwelling birds, this difference in performance suggests that birds may generate sub-maximum power during steady flight, with substantial reserve capacity for escape behaviors. For flying insects, a comparison between optimized and realized power output is available for the asynchronous (fibrillar) wing elevator muscles of bumble bees (Josephson and Ellington, 1997; Josephson, 1997). These muscles undergo length oscillations near the frequency that maximizes power output, but the *in vivo* strain amplitude is suboptimal for maximal power generation. These particular characteristics could be related to specializations for stretch activation (Machin and Pringle, 1960; Josephson et al., 2000).

Among insects with synchronous flight muscles, the conditions that maximize power output have been well documented in hawkmoths (Stevenson and Josephson, 1990), locusts (Mizisin and Josephson, 1987) and katydids (Josephson, 1985a,b). These studies, however, do not address the extent to which optimized experimental conditions match the full set of *in vivo* operating conditions.

The mesothoracic dorsolongitudinal muscles (dl_1 muscles; nomenclature of Nüesch, 1953) of the hawkmoth *Manduca sexta* provide an advantageous system in which to compare potential *vs* realized performance. The dl_1 muscles are the largest muscles in the moth, comprising 5–8% of the total body mass. Because these synchronous muscles are typically activated only once in each wing stroke (Kammer, 1967), the timing of activation can be unambiguously determined from extracellular muscle recordings. During flight, the dl_1 muscles function exclusively to generate most if not all of the mechanical power used to depress the wings. Optimization of the dl_1 muscles for maximum power output would therefore be consistent with their role as the major source of aerodynamic power. In a previous study (Tu and Daniel, 2004), we determined the *in vivo* operating conditions of the dl_1 muscles of *Manduca* during steady state tethered flight. Here, we determine the extent to which power generation is maximized in a synchronous insect flight muscle by comparing the maximum potential power output of the dl_1 muscles to their power output realized under *in vivo* operating conditions.

Materials and methods

Animals and muscles

Adult *Manduca sexta* L. were obtained from a colony maintained in the Department of Biology at the University of Washington. Larvae were raised on artificial diet at 26°C. Both larvae and adults were maintained under a 17 h:7 h L:D photoperiod. We shifted the photoperiod of the moths so that the onset of their dark period occurred in mid-morning. Adults were used within 1–3 days of eclosion.

The dl_1 muscles span the length of the mesothorax and attach to the 1st and 2nd phragmata (Fig. 1B). The phragmata are deep invaginations of the dorsal exoskeleton that form broad areas for muscle attachment. Each of the bilaterally paired dl_1 muscle consists of five subunits, designated, from ventral to dorsal, dl_{1a} to dl_{1e} (Nüesch, 1953; Eaton, 1988).

Force transducer

The force transducer consisted of a cantilevered 6.25 mm×1.5 mm brass beam with a free length of 35.25 mm. We used an optical sensor (Spot 2D, UDT Sensors Inc., Hawthorne, CA, USA) to track the position of a short length of stainless steel hypodermic tubing soldered to the end of the beam. The force beam had a compliance of 3.6×10^{-4} mm mN^{-1} and an unloaded resonant frequency of 640 Hz. The force transducer was mounted on a 3-axis micromanipulator, which in turn was mounted on a linear translation stage. Using the calibrated micrometer on the translation stage, we could adjust the force transducer position with a precision of 0.01 mm. A custom-built PID controller used the outputs of the optical length sensor and the voltage-controlled oscillator as comparator signals. This feedback circuit minimized variation in length changes as we varied either amplitude or stimulus phase.

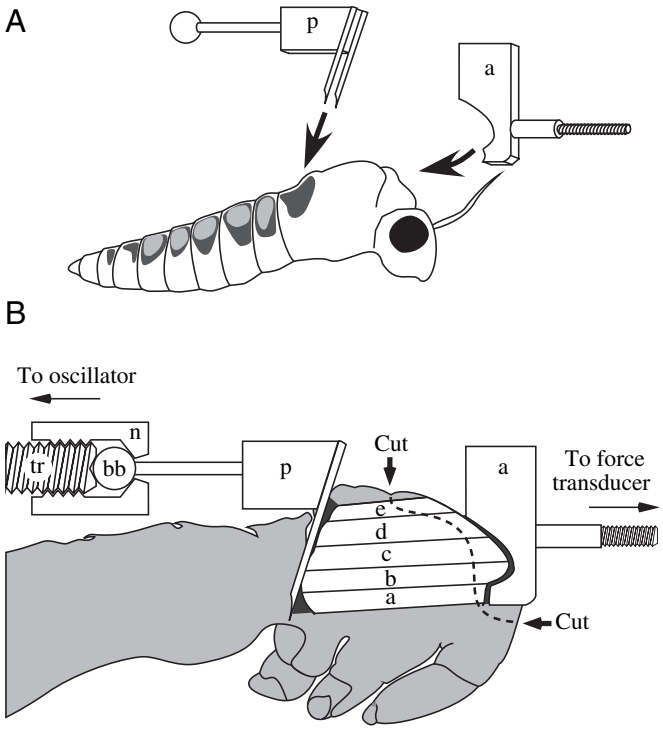

Fig. 1. Muscle preparation for work loop measurements. (A) Placement of the anterior (a) and posterior (p) muscle grips for force measurements on mechanically isolated muscles. (B) After decapitating the moth, the 1st phragma was exposed and the anterior grip placed over the anterior insertion of the dl_1 muscles. The paired needles of the posterior grip were driven through the dorsal cuticle and down along the posterior face of the 2nd phragma. Both grips were secured to the exoskeleton with cyanoacrylate adhesive. After gluing acetate strips (not shown) across the gap between the two grips to fix their relative positions, cuticle strips were excised (arrows, broken line) to mechanically isolate the anterior grip and muscle insertions from the rest of the thorax. The anterior grip was then secured to the force transducer *via* the treaded rod projecting from the grip. The ball bearing (bb) mounted on the posterior grip fit into a depression in the end of a threaded rod (tr) mounted on a magnetic coil oscillator. When secured by a slotted retaining nut (n), the ball bearing and threaded rod formed a ball joint. The acetate strips spanning the two grips then were cut, and any misalignment of the cut ends was corrected using the ball joint and oscillator. a–e, dl_1 muscle subunits.

Muscle length oscillation

Sinusoidal length changes were imposed on the muscle using a magnetic coil oscillator (V200 series, Ling Dynamic Systems, Yalesville, CT, USA), modified with a leaf spring to increase its unloaded stiffness. To measure muscle length changes, we used an optical sensor (LSC 30D, UDT Sensors

Inc., Hawthorne, CA, USA) to track the position of a red LED attached to the shaft of the oscillator.

Temperature

We measured thoracic temperature to the nearest 0.1°C using a 0.15 mm diameter copper-constantan thermocouple inserted into the dl_1 muscle through a small hole in the exoskeleton. The entire experimental apparatus was enclosed within an insulated plywood box. Heated water circulating through copper pipe within the box maintained the muscle temperature at 36±0.5°C.

Muscle stimulation

We elicited twitches using bipolar, supramaximal stimuli, 0.2 ms in duration, delivered through a pair of electrodes formed from stainless steel minuten pins. The electrodes were inserted through the anterior notum and into the dl_1 muscle, one on either side of the midline.

Muscle preparation

The dl_1 muscles receive their primary respiratory air supply from large tracheal trunks originating at the mesothoracic spiracles. On each side of the moth, these tracheal trunks run anteriorly between the dl_1 muscles and the dorsoventral muscles, supplying both muscle groups. This arrangement of tracheae made it impossible to remove the dl_1 muscles from the thorax without compromising their oxygen supply. In addition, respiratory pumping by the abdomen appears critical for prolonged viability of the dl_1 muscles; muscle performance deteriorated rapidly if we removed the abdomen in order to expose the posterior muscle attachments on the 2nd phragma. We therefore developed a semi-intact preparation that minimized the dissection necessary to mechanically isolate the dl_1 muscles between two specially constructed grips.

The anterior grip consisted of a small aluminum block shaped to match the contours of the anterior mesoscutum and the 1st phragma (Fig. 1A). After being weighed, each moth was decapitated, its legs and wings removed, and the scales rubbed off the dorsal surfaces of the thorax. The 1st phragma was exposed by severing the pronotum near its articulation to the mesothoracic prescutum and by clearing away the prothoracic dorsolongitudinal muscles. After scraping away the waxy epicuticle, we used cyanoacrylate adhesive to attach the grip to the cuticle overlying the anterior origins of the dl_1 muscles. Any gaps between the grip and the exoskeleton were filled with a composite formed from cyanoacrylate and sodium bicarbonate powder.

The posterior grip consisted of a pair of 0.68 mm diameter stainless steel hypodermic needles soldered to a small brass block (Fig. 1A). The needles were parallel to each other and were separated by a distance slightly less than the lateral width of the 2nd phragma. A drop of cyanoacrylate adhesive was placed in the deep groove overlying the phragma. We then pushed the needles down into the groove so that they punctured the metathoracic scutellum and passed down along the posterior face of the phragma (Fig. 1A). Cyanoacrylate flowing between the needles and the cuticle solidly bonded the phragma and scutellum to the needles and brass block (Fig. 1B). We discarded trials if dissection following the measurements showed that the needles had pierced the phragma, or if the needles and phragma were not solidly bonded.

To preserve the orientation of the dl_1 muscles as the thorax was transferred to the experimental apparatus, we glued two strips of acetate transparency film, one strip on each side, across the gap separating the two grips. The acetate strips restricted length changes and minimized bending and torsion of the muscles. We then mechanically isolated the dl_1 muscles from the thoracic exoskeleton by excising a thin strip of cuticle from around the anterior grip (Fig. 1B).

The anterior grip was attached to the force beam *via* a short, threaded steel rod projecting from the front of the grip (Fig. 1B). The threaded end of the rod was inserted through a hole near the end of the force beam and secured with a nut. The posterior grip was attached to the shaft of the magnetic coil oscillator *via* a short length of stainless steel tubing projecting from the back of the grip. The tubing terminated in a ball bearing, which fitted into a depression in the end of the oscillator shaft, and formed a ball joint when secured with a slotted retaining nut.

Once the two grips were secured, we cut the acetate strips connecting the two grips. The dl_1 muscles then formed the only direct mechanical linkage between the oscillator and the force beam. We used the ball joint and the micromanipulator mount of the force beam to restore the initial muscle length and orientation. The position of the muscle was adjusted until the cut edges of the acetate strips were just touching and exactly aligned. The force beam manipulator was then locked in position and the retaining nut on the oscillator shaft was tightened to prevent movement of the posterior grip relative to the oscillator shaft. Finally, the acetate strips were trimmed away to prevent mechanical interference with imposed muscle length changes.

Muscle length, mass and cross-sectional area

The length L_{max} at which the dl_1 muscles generate their maximum isometric twitch force provides a reliable physiological reference length that is independent of the experimental method and of any offsets introduced in the initial preparation. We therefore referenced previous measurements of *in vivo* operating length and strain amplitude to L_{max} (Tu and Daniel, 2004), and we continue the procedure here. However, because of the internalized skeletal attachments of the dl_1 muscles, we could not measure the absolute value of L_{max} until after completing all of our work loop measurements. To solve this difficulty, we first performed a series of length–tension measurements to determine the position of L_{max} relative to the initial muscle length. We then calculated values for experimental length offsets and strain amplitudes based on an average value of L_{max} determined from a series of preliminary length tension measurements.

To measure the position of L_{max} relative to the initial muscle

length, we performed a series of isometric twitch length–tension measurements on each muscle prior to measuring power output. At each length, the muscle received five supramaximal stimuli at 1 Hz. We changed the muscle length during a 5 s interval separating each burst of stimuli. Starting at a length 0.4 mm shorter than the initial length, we increased length in steps of 0.1 mm up to 0.2–0.3 mm beyond our estimate of L_{max}. We then repeated the length series in reverse order. From the average twitch amplitude at each length step, we identified L_{max} for the ascending and descending length series. If the two series gave different values of L_{max}, we used the average of the two values.

At the conclusion of each experiment, we dissected the thorax to expose the dl_1 muscles. We first used the calibrated micrometer on the translation stage to return the dl_1 muscles to their initial length. Two strips of stainless steel shim, one on each side, were glued across the gap separating the grips, securing the muscle at its initial length. We then removed the preparation from the experimental apparatus. The dl_1 muscles of one side were dissected free of the thorax and placed in *Manduca* saline (Tublitz and Truman, 1985). We then recorded a video image of the medial aspect of the intact, contralateral dl_1 muscles. The remaining dl_1 muscles were then dissected free of the thorax and placed in saline. Immediately afterwards, we blotted the muscles and weighed them together to the nearest 1 mg.

The absolute value of L_{max} was calculated from the recorded offset between the initial length and L_{max}, and the distance between the ventral margins of the 1st and 2nd phragma, measured on the video image. We previously defined the *in vivo* operating length, L_{op}, to be the median length of dl_{1a} during flight (Tu and Daniel, 2004). By mapping length changes of the dl_1 muscles onto their isometric twitch length-tension curve, we found that on average, L_{op} was equal to $0.89L_{max}\pm0.04$ (mean ± S.D.; Tu and Daniel, 2004). Using the specific value of L_{max} for each muscle, and this average value of L_{op} relative to L_{max}, we calculated an estimate of L_{op} for each muscle.

Muscle volume was calculated from the measured muscle mass, assuming a muscle density of 1 g cm^{-3}. Muscle fiber length measurements were taken on the video image of the medial surface of the dl_1 muscles on one side. We calculated an average fiber length from six measurements taken at locations that were evenly distributed between the dorsal and ventral margins of the muscle.

Timing and phase of muscle activation

In our recordings of *in vivo* muscle activation and length changes during tethered flight (Tu and Daniel, 2004), we calculated the phase of activation of the dl_1 muscle as the time from the start of muscle lengthening to the peak of the spike in the subsequent extracellular spike, divided by the cycle period. Here we applied these measurements of *in vivo* activation phase to power measurements on isolated muscles. To do so, we first had to account for a possible difference in the timing between spikes in extracellular muscle recordings, and stimuli delivered to the muscle through extracellular electrodes. We therefore performed a series of measurements using muscle preparations identical to those used for power measurements, with the addition of bipolar extracellular recording electrodes implanted in the right dl_{1c}, as described in Tu and Daniel (2004). For each preparation, we recorded evoked extracellular potentials during trains of supramaximal stimuli delivered at 1 Hz. We performed signal averaging of successive responses using the stimulus as a time reference, and measured the delay between the onset of the stimulus and the peak of the evoked muscle potential (Fig. 2). We define the phase of activation in our work loop measurements as the projected time of the evoked potential following an applied stimulus, normalized to the cycle period: phase=$(\Delta t_s+\Delta t_{ep})/P$, where Δt_s is the delay from the onset of muscle lengthening to the onset of the applied stimulus, Δt_{ep} is the average delay between the onset of the stimulus and the peak of the evoked muscle potential, and P is the cycle period.

Experimental protocols

During flight, *Manduca* regulate their internal thoracic temperature in the range of 32–42°C (Heinrich, 1971; Heinrich and Bartholomew, 1971; McCrea and Heath, 1971), and have a wing stroke frequency of approximately 25 Hz (Willmott and Ellington, 1997). In all trials, therefore we held muscle temperature and cycle frequency constant at 36±0.5°C and 25 Hz, respectively, and systematically varied the phase of activation, mean length and strain amplitude. The range of experimental variation in each of these parameters was sufficient to include both the *in vivo* value, and the value that gave the maximum mechanical power output. Each combination of parameters was tested at three strain amplitudes, with peak-to-peak values normalized to the estimated value of L_{op}, approximately 0.10, 0.075 and 0.05. Together with any experimental length offsets, all amplitudes were determined precisely for each individual after all power measurements were complete. For each measurement of power output, the muscle was subjected to a burst of 25 cycles of stimulation combined with sinusoidal length changes imposed symmetrically around an experimental length. Experimental parameters were adjusted to new values during the 5 s that separated each burst. We performed two sets of measurements of mechanical power output, one to examine the effects of stimulus phase, and the second to focus on the effects of mean muscle length.

Our first set of measurements focused on the effects of stimulus phase on power output. For each of the three amplitudes tested, we performed measurements at four experimental lengths: L_{max}, the initial muscle length L_0, and two intermediate lengths. At each experimental length, a complete phase series consisted of power measurements at 19 values of stimulus phase, evenly spaced throughout the length cycle in fractional increments of 0.05. The three amplitudes were tested in increasing order. Within each amplitude set, the order in which the four experimental lengths was randomized, as was the order of phase values within each length series.

Randomization was performed separately for each animal prior to the start of the measurements (rand.m, Matlab v.4, The Math Works Inc., Natick MA USA), and the randomized length and phase sequences were programmed into the software controlling the work loop measurements. The 228 measurements of the 12 experimental series (three amplitudes, each at four experimental lengths) required approximately 50 min to complete.

We performed a second set of measurements to examine power output in greater detail over a restricted range of phase and a greater range of experimental lengths. We employed five values of stimulus phase, evenly spaced at fractional increments of 0.05. These values encompassed both the phase measured *in vivo* and the optimum stimulus phase for power output determined from the first set of work loop measurements. We performed three series of measurements on each muscle, one at each strain amplitude. Each series started with the muscle length set to 0.1–0.2 mm shorter than the estimated value of L_{op}. At each length, the muscle was given five bursts of stimulation and sinusoidal length change. Randomization of the phase presentation at each length was performed as described for the first set of measurements. We then increased the experimental length by 0.1 mm, and repeated the measurements at the five phase values. Each of the three length series consisted of 100 measurements at 20 length steps and five phase values, for a total of 300 measurements on each preparation.

Force and length data were both digitized at a rate of 5 kHz, and digitally low-pass filtered with zero phase delay and a cutoff frequency of 400 Hz. We calculated the net work performed per cycle by integrating force with respect to muscle length over the last five complete cycles of each burst. Power was calculated as the product of the net work per cycle and the cycle frequency. Values are given as means ± 1 S.D.

Results

Timing of muscle activation

In four moths, the average delay Δt_{ep} between the stimulus and the peak of the evoked muscle potential was 5.9±1.4 ms (Fig. 2).

Muscle length at L_{max}

The mean value of L_{max} determined from a series of length tension measurements on six muscles was 12.3±1.13 mm.

Muscle power output

We measured power output from a total of six muscle preparations, three to examine the effects of the phase of activation and three to examine the effects of experimental length. The six moths used for work loop measurements were all females with a mean body mass of 2.75±0.029 g. The left and right dl_1 muscles from these moths had a mean combined mass of 0.164±0.017 g, a mean combined cross sectional area of 21.58±2.51 mm^2, and a mean mean fiber length of 7.63±0.40 mm. The three strain amplitudes used in all six preparations had mean values of 5.0±0.4L_{op}, 7.7±0.4L_{op}, and 10.3±0.6L_{op}. We calculated distortion of the imposed sinusoidal length changes as the amplitude of the 2nd harmonic of the Fourier power spectrum, expressed as a percentage of the 1st harmonic. The mean distortion averaged across all measurements was 7.0±1.7% (Fig. 3). The magnitude of isometric twitch forces, measured at the beginning and at the end of each preparation, declined by 13.7 to 19.2% during the hour required to complete the series of measurements on each muscle. Because we randomized the order of the length, phase and strain amplitude, this decline in performance should not have introduced a systematic bias in our results. Within all of the power measurements, the largest discrepancies between initial and final values of muscle stress and length over a segment of five cycles were 3.8% and 1.4%, respectively.

In the first three preparations, at each experimental length and strain amplitude, power output varied through a single maximum and a single minimum value as we changed the phase of activation from 0 to 1 (Fig. 4). All three muscles generated positive power output between fractional phase values of 0.2 and 0.6, and maximal power between 0.3 and 0.4. Both the magnitude of the peak positive power output and the peak rate of energy dissipation (negative power) increased with increasing strain amplitude. Average values of the four experimental lengths, normalized to L_{op}, were 0.97±0.01, 1.01±0.01, 1.05±0 and 1.12±0. Positive power output was consistently lower at the shorter two lengths, which were also the lengths closest to the *in vivo* operating length. In all cases, differences in power output due to changes in strain amplitude and experimental length were small compared to differences due to changes in the phase of activation.

The experimental lengths tested using the second group of three muscle preparations fell in the range of 0.95±0.01L_{op} to 1.17±0.01L_{op}. Based on the results of the first three preparations, we used five values of fractional phase between 0.3 and 0.55. At each of the three amplitudes tested, these values of phase and length were sufficient to resolve a distinct maximum in power output while including the values of phase and length measured *in vivo* (Fig. 5). The maximum power output increased with strain amplitude, although the difference between the maximum power output at the two higher amplitudes was consistently small.

The dl_1 muscles of all six preparations generated a mean maximum power output of 83.3±13.2 W kg^{-1} (Table 1). On average, the dl_1 muscles generated maximum power output at a phase of 0.36±0.03, an experimental length of 1.11±0.05L_{op}, and a strain amplitude of 0.092±0.011L_{op}.

We based our estimate of *in vivo* power output on a subset of measurements taken using experimental parameters that most closely matched the *in vivo* operating conditions measured by Tu and Daniel (2004). For each of the six muscle preparations, we first identified measurements taken at phase values within one standard deviation of the mean phase measured *in vivo* (0.49±0.04). We further reduced this data set by selecting measurements taken at lengths (0.96–1.05L_{op}) within one standard deviation of the mean *in vivo* operating

length. Finally, we selected the subset of measurements taken at strain amplitudes between $0.08L_{op}$ and $0.10L_{op}$. This range of amplitudes was well within the range of strain amplitudes measured *in vivo* ($0.055L$–$0.013L_{op}$; mean $0.09\pm0.02L_{op}$; Tu and Daniel, 2004). The mean power output from all six preparations measured under *in vivo* conditions was 47.4±11.3 W kg^{-1} (Table 2). This power output was measured at a mean phase of 0.48±0.01, a mean experimental length of 1.01±0.01 and a mean strain amplitude of $0.086\pm0.005L_{op}$. Under *in vivo* conditions the dl_1 muscles generated only 57% (range: 40–67%) of their maximum potential power output (Table 2, Fig. 5). Using the same search procedure, the mean power output at the maximum and minimum values of phase measured *in vivo* (Tu and Daniel, 2004) was 29.9±11.5 W kg^{-1} at phase values of 0.56±0.03, and 65.3±12.8 W kg^{-1} at phase values of 0.45±0.02. This range corresponds 35.7–77.9% of the maximum power output measured in this study. The strain amplitude that maximized power output in our measurements was similar to the measured *in vivo* strain amplitude. However, relative to the mean *in vivo* phase of activation, the phase that maximized power output was advanced by 12% of the cycle period, and the length that maximized power output was 10% longer than the *in vivo* operating length. With changes in the phase of activation, power output varied as a result of changes in the size of the work loops, without any lemniscate behavior in the force–length trajectories (Fig. 6).

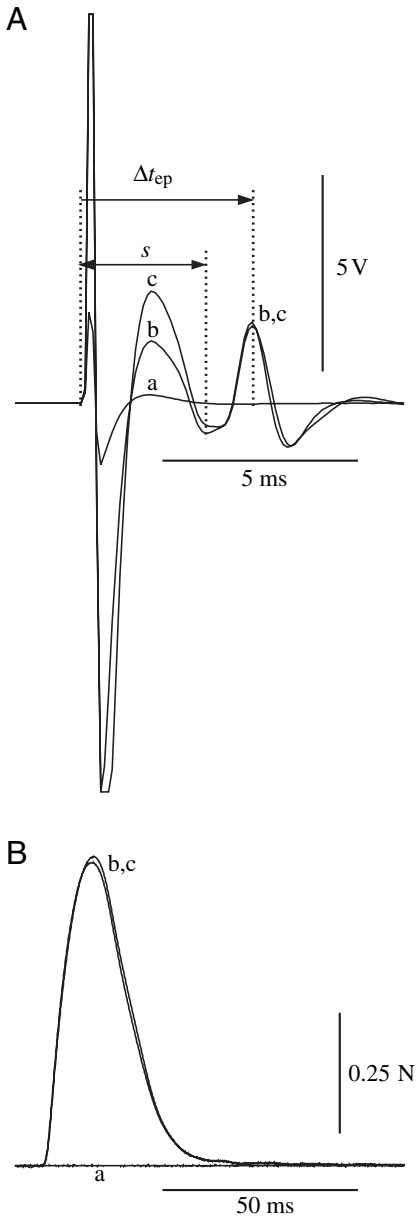

Fig. 2. To adjust for the difference in timing between a stimulus applied to the muscle and muscle activation recorded during tethered flight, we recorded extracellular potentials (A) and force (B) from the dl_1 muscles during isometric twitches. Stimuli were delivered through extracellular electrodes spanning all subunits of the dl_1 muscles and were 0.2 ms in duration. Extracellular potentials were recorded from dl_{1c}. (A) Three extracellular muscle potentials in response to stimuli of increasing amplitude. The stimulus artifact (*s*) varied in amplitude with the amplitude of the applied stimulus. Subthreshold stimuli (a) produced only a stimulus artifact whereas suprathreshold stimuli (b,c) resulted in a clearly identifiable extracellular spike of constant amplitude. We defined the delay between the onset of the stimulus and the evoked potential (Δt_{ep}) as the time between the onset of the stimulus artifact and the peak of the evoked potential. The large voltage deflections of the stimulus artifact in b and c exceeded the range of the data acquisition system and are cut off at ±10 V. (B) Muscle force recorded following the three stimuli shown in A. Note that the time scale differs from that in A. Subunits of the dl_1 muscles responded in an all-or-none manner to stimuli. Subthreshold stimuli (a), defined by the absence of an evoked extracellular spike, generally did not result in twitch forces. Supramaximal stimuli (b,c) consistently produced a maximal twitch of nearly constant amplitude. In some preparations, subthreshold stimuli evoked submaximal twitches with discreet amplitudes. In these cases, the submaximal twitches probably resulted from selective recruitment of subunits other than dl_{1c}, the subunit in which we had implanted the recording electrodes. Stimulus amplitude in our measurements of mechanical power output was adjusted to the level that produced the maximal twitch force from the whole muscle. We defined the phase of activation in our work loop measurements as the projected time of the evoked potential normalized to the cycle period (see text for details).

Discussion

Our measurements of mechanical power output from the dl_1 muscles of *Manduca* are the first direct comparisons of *in vivo* and optimized performance for a synchronous insect flight muscle. At a cycle frequency of 25 Hz and at 36°C, the average maximum power output from the dl_1 muscles, 83 W kg^{-1}, falls within the range of maximal power output previously reported for a dorsoventral muscle of *Manduca* at 28 Hz: 80 W kg^{-1} at 35°C and 90 W kg^{-1} at 40°C (Stevenson and Josephson, 1990). Maximal power output from the dl_1 muscles was also similar to values reported for other synchronous insect muscles: a metathoracic wing elevator muscle from two species of locust (72–73 W kg^{-1}; Mizisin and Josephson, 1987) and from a katydid (76 W kg^{-1}; Josephson, 1985a), and the basalar muscle of a dragonfly (91–124 W kg^{-1}; Marden et al., 2001). However,

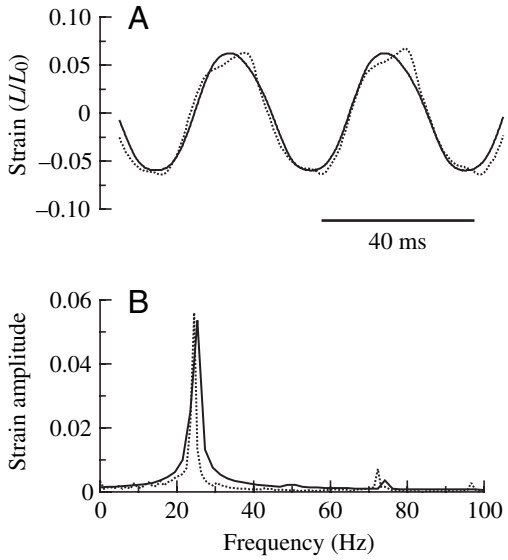

Fig. 3. Sinusoidal length changes replicated the major components of the *in vivo* strain trajectory. (A) Two cycles of length change from work loop measurements (solid lines) and from tethered flight (dotted lines, from Tu and Daniel, 2004) chosen on the basis of their closely matching frequency and amplitude. Trajectories recorded during tethered flight matched sinusoidal length changes through most of the cycle but were typically more complex at the transitions from lengthening to shortening. (B) Fourier spectra calculated from the two records shown in A. Sinusoidal length changes replicated the dominant characteristics of the length changes recorded in tethered flight.

under conditions that replicated *in vivo* length, strain trajectory, cycle frequency, activation timing and temperature, the dl_1 muscles achieved only 40–67% of their maximum potential mechanical power output. Both the *in vivo* phase of activation and the *in vivo* operating length differed substantially from values that maximized power output. Submaximal power output from the dl_1 muscles is surprising since these muscles generate most if not all of the power for the downstroke, and therefore a large fraction of the mechanical power for flight. In the following discussion, we first address possible sources of error in our measurements. We then discuss possible implications of submaximal power output for our understanding the design of musculoskeletal systems.

Assessment of in vivo *power output*

Assessment of *in vivo* power output requires accurate replication of the *in vivo* operating parameters of a muscle (Marsh and Olson, 1994). Our experimental protocol reproduced the *in vivo* values of temperature, cycle frequency, phase of activation, mean muscle length and strain amplitude previously reported for *Manduca* (Heinrich, 1971; Heinrich and Bartholomew, 1971; McCrea and Heath, 1971; Willmott and Ellington, 1997; Tu and Daniel, 2004). Two other variables, the strain distribution within the dl_1 muscles, and the shape of the strain trajectory, were the most potentially troublesome to replicate in the isolated muscle.

Although our experimental methods minimized any initial distortion of the dl_1 muscles, localized strains within the muscle during imposed length changes may have differed from the strain distribution *in vivo*. Josephson and Ellington (1997) suggested that strain amplitudes within bumblebee flight muscle might be uniform, but the actual spatial distribution of muscle fiber strain has yet to be mapped in *Manduca* or in any other insect. Lacking such data, we applied uniform length changes to the whole muscle. Differences in fiber length among the five subunits of the dl_1 muscles necessarily produced local variation in strain. Our data show that the magnitude of power output at a given phase varies with strain amplitude, suggesting that inhomogeneous strains within the muscle could in fact affect our measurements of total power output. We based the imposed length changes, however, on those measured directly from subunit dl_{1a}, the largest subunit of the dl_1 muscles, and the subunit with the largest lever arms on the 1st and 2nd phragmata. This protocol should have minimized errors in strain amplitude within dl_{1a}, and the power output of this subunit should dominate the performance of the muscle as a whole. More importantly, we have no evidence to suggest that strain inhomogeneities could have altered the relationship between power output and the phase of activation. Because all subunits of the dl_1 muscles are mechanically coupled, local gradients in strain could not have produced local differences in the phase of activation. In addition, the phase of activation that maximized power output did not change with strain amplitude (Fig. 4). It is therefore unlikely that we would measure peak power output at the *in vivo* phase of activation, even if we were to precisely replicate the fine scale distribution of strain amplitudes within the muscle.

Our use of sinusoidal motions to approximate *in vivo* length changes represents an additional potential complication. Asymmetrical triangle strain trajectories with prolonged shortening can augment power output relative to that generated during sinusoidal length oscillations (Askew and Marsh, 1997; Girgenrath and Marsh, 1999). Length changes of the dl_1 muscles, however, did not show appreciable asymmetries between the duration of lengthening and shortening (Tu and Daniel, 2004). For symmetrical strain trajectories, the available evidence suggests that even fairly substantial variation in trajectory shape does not greatly alter the net power output. Josephson (1989) used a mathematical model to predict that muscles would perform similar amounts of work during both sinusoidal and triangle wave length changes. This result has been confirmed experimentally for muscles undergoing sinusoidal and triangle length oscillations with equal shortening and lengthening duration (Askew and Marsh, 1997). During swimming, the natural strain trajectory of the scallop adductor muscle departs strongly from either a simple sinusoidal or triangle waveform. The net power output of the adductor muscle, however, is similar during both sinusoidal and natural strain cycles (Marsh et al., 1992; Marsh and Olson, 1994). These results suggest that the comparatively small discrepancies between the applied and *in vivo* length changes in our measurements did not greatly affect the magnitude of our measured power output.

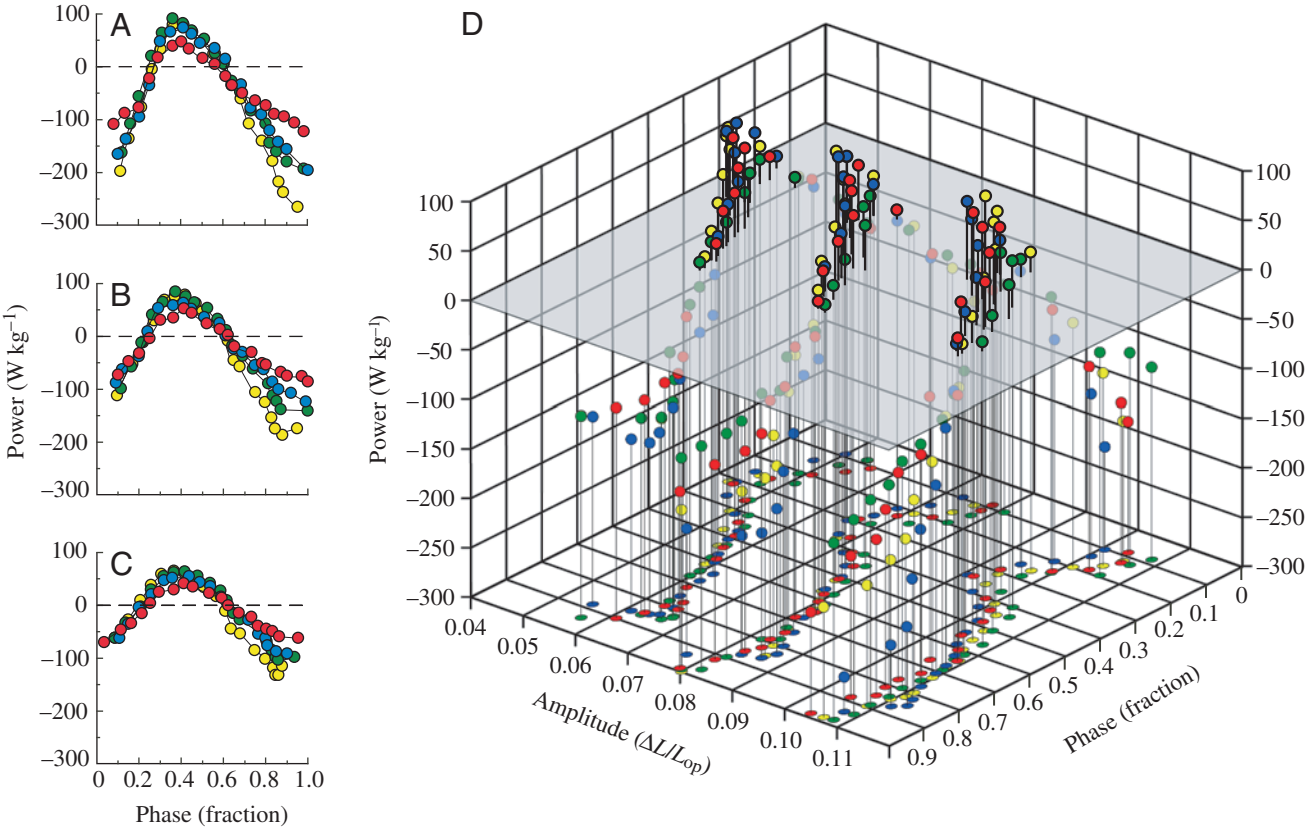

Fig. 4. Mechanical power output is plotted against the phase of muscle activation at four mean experimental lengths, and three strain amplitudes. The data shown are from one muscle preparation (Moth 1 in Tables 1, 2). (A–C) The muscle was subjected to length oscillations at three experimental strain amplitudes with mean values of 0.105±0.0053L_{op} (A), 0.078±0.0058L_{op} (B), and 0.049±0.0143L_{op} (C) (N=76 for each amplitude). At each amplitude setting, we imposed muscle length changes symmetrically around four experimental lengths: 0.98L_{op} (red), 1.02L_{op}(blue), 1.05L_{op}(green), and 1.12L_{op}(yellow). We measured mechanical power output at each combination of amplitude and experimental length as we varied the phase of activation through the strain cycle in 19 evenly spaced increments, expressed as a fractions of the cycle period. (D) Combined data from A–C. Limitations of our feedback controller resulted in some variation in strain amplitude within any one sweep of phase values. The effects of changes in strain amplitude and experimental length were small compared to the variation in mechanical power output with changes in the phase of activation. At each combination of strain amplitude and experimental length, power varied through a single maximum and minimum as we changed the phase of activation from 0 to 1. Power was positive between phase values of 0.2 and 0.6, and maximal between 0.3 and 0.4. With increasing amplitude, both the magnitude of the peak positive power output as well as the peak rate of energy dissipation (negative power) increased. Positive power output was consistently lowest at the experimental lengths (0.98L_{op} (red), and 1.02L_{op} (blue)) that were closest to the *in vivo* operating length.

Our assessment of *in vivo* power output would be most seriously in error if the discrepancies between the applied and *in vivo* strain trajectories were sufficient to shift the phase of activation that maximized power output. Variation within and among individuals complicates exact replication of the *in vivo* strain trajectories. Neither an exact replica of the strain measured from one individual, nor an average strain trajectory compiled from multiple individuals would have been entirely appropriate for any one muscle. Sinusoidal length changes, however, did in fact replicate the dominant features of the strain trajectory common to all of our *in vivo* measurements (Fig. 3). Our applied sinusoidal length changes lacked the higher frequency components contained in the *in vivo* strain waveform at roughly twice wingstroke frequency (Fig. 3; Tu and Daniel, 2004). It is unlikely, however, that the inclusion of this missing component would be sufficient to augment the power output at the *in vivo* length and phase of activation by the 40 W kg^{-1} necessary to match the maximum measured power output. Gilmour and Ellington (1993) examined the effect of including the second harmonic from the *in vivo* strain waveform in the driving signal for *in vitro* work loop measurements. In glycerinated fibers from the asynchronous flight muscles of bumblebees, inclusion of the second harmonic generally reduced the net power output. Although these results suggest that purely sinusoidal strain trajectories might overestimate *in vivo* power output, there are currently no published studies bearing on the consequences of the sequential addition or subtraction of the Fourier components of a complex strain trajectory of synchronous muscle. Without such data, it is difficult to assess the importance of subtle

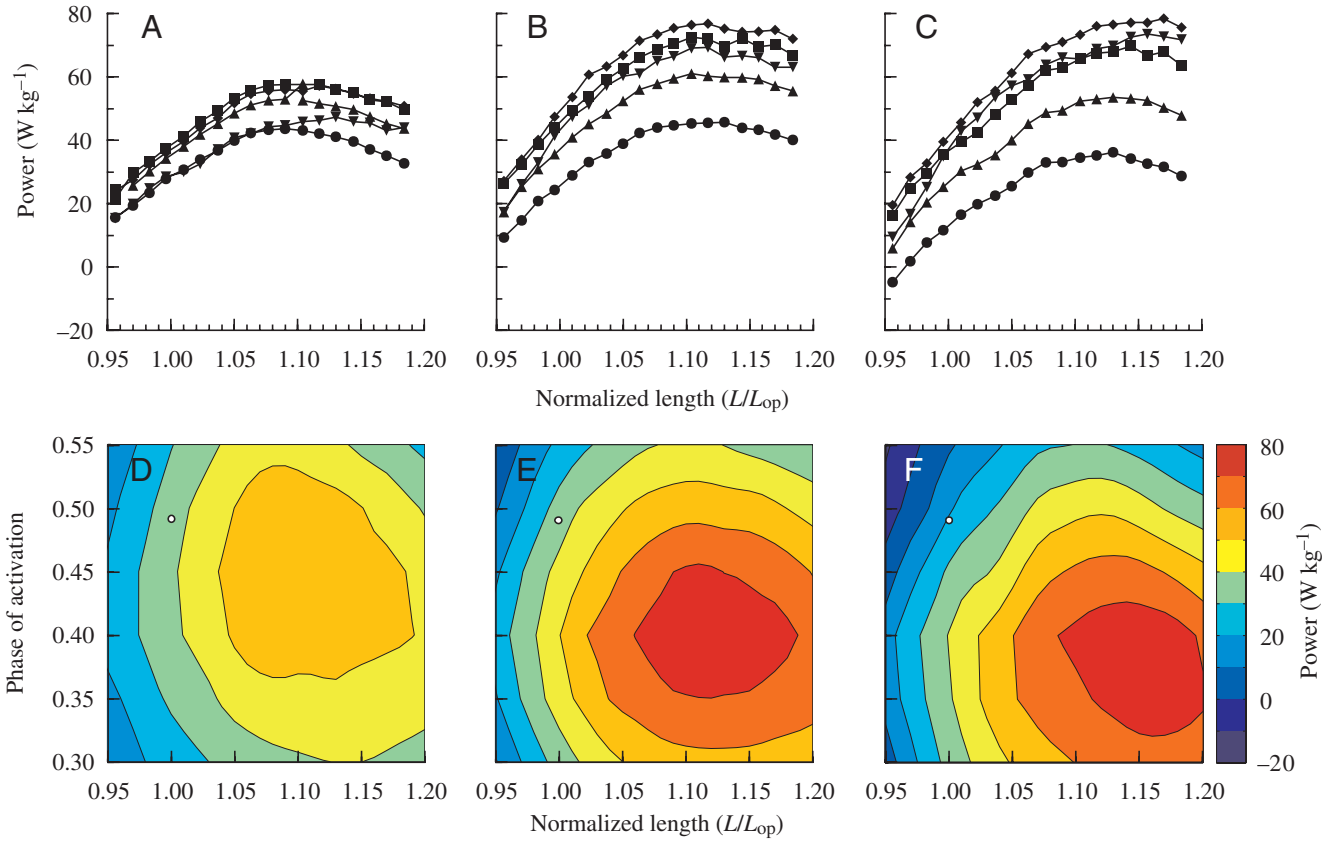

Fig. 5. Power output of the dl_1 muscles is plotted over a range of activation phases, experimental lengths and strain amplitudes that encompass both peak power and *in vivo* operating conditions. (A–C) Variation in mechanical power output as a function of experimental length. Experimental length is normalized to operating length. Each plot shows measurements taken at one peak-to-peak strain amplitude normalized to L_{op}: (A) 0.048, (B) 0.083, (C) 0.115. Within each plot, each curve shows data from measurements at one of five values of the phase of activation: ▼ 0.31, ◆ 0.37, ■ 0.42, ▲ 0.47, ● 0.52. At each amplitude power output was consistently lowest at the phase values (0.47 and 0.52) that were closest to the phase of activation measured *in vivo* (0.49±0.04; Tu and Daniel 2004). (D–F) Contour plots showing power output, coded by color, as a function of the phase of activation and experimental length. Each plot is based on 90 measurements of power taken at five values of activation phase and 18 values of experimental length. The contour lines were fitted to the data by interpolation using an inverse distance method (griddata.m, Matlab v.4, The Math Works Inc., Natick MA USA). Each plot shows measurements taken at one peak-to-peak strain amplitude, normalized to L_{op}: (D) 0.048, (E) 0.083, (F) 0.115. At all three amplitudes, power output near the values of operating length and phase of activation measured *in vivo* (open circle) was substantially lower than the peak power output. The mean strain amplitude measured *in vivo* (0.090±0.031L_{op}) lies between the amplitudes tested in B,C, and E,F. Data in A–F are from one muscle preparation (Moth 6 in Tables 1, 2).

complexities in the *in vivo* strain trajectory for our data, or to draw generalized conclusions from specific measurements of power output made under more complex strain regimes.

In vivo *power output and muscle function*

From recent studies, it is now clear that in addition to power generation, muscles used in terrestrial locomotion serve a variety of functions, such as braking (Full et al., 1998; Ahn and Full, 2002), energy storage (Roberts et al. 1997; Biewener et al., 1998) and energy transmission (Olson and Marsh, 1998). It is further evident that these additional functions can conflict with maximum power generation. During swimming and flying, however, the absence or relaxation of these additional demands could permit greater optimization of muscle function for maximum power. Surprisingly, maximal power output by the red muscle of skipjack tuna currently stands as the lone example of such optimization for swimming fish (Syme and Shadwick, 2002). Submaximal power output by the propulsive muscles of other fish suggests that, as in terrestrial locomotion, multiple functions such as energy transmission and stabilization of the body may compromise power output in swimming (Altringham et al., 1993; Hammond et al., 1998; Rome et al., 1999; Coughlin, 2000; Swank and Rome, 2001).

Among flying insects, submaximal power output by both the asynchronous flight muscles of bumblebees (Josephson, 1997) and the synchronous dl_1 muscles of *Manduca* suggest that insect flight muscles may also operate under constraints that compromise their ability to generate maximal power under *in vivo* conditions. For *Manduca*, the indirect mechanical linkages between the dl_1 muscles and the wing hinge clearly do not indicate a major role in the stabilization and control of flight. These functions almost certainly reside primarily in the small, laterally placed, flight muscles, which insert directly onto elements of the wing articulation (Kammer, 1971;

Table 1. *Summary of the maximum power output measured from each moth, together with the corresponding values of phase, experimental length and strain amplitude*

Moth	Power (W kg^{-1})	Phase (fraction)	L_e	Strain amplitude
1	91.0	0.34	1.05	0.095
2	86.2	0.37	1.05	0.071
3	93.8	0.39	1.12	0.094
4	91.7	0.39	1.15	0.093
5	58.7	0.33	1.12	0.093
6	78.4	0.37	1.17	0.106
Mean	83.3±13.2	0.36±0.03	1.11±0.05	0.092±0.011

Experimental length, L_e, is normalized to the operational length, L_{op}. Values are means ± 1 S.D.

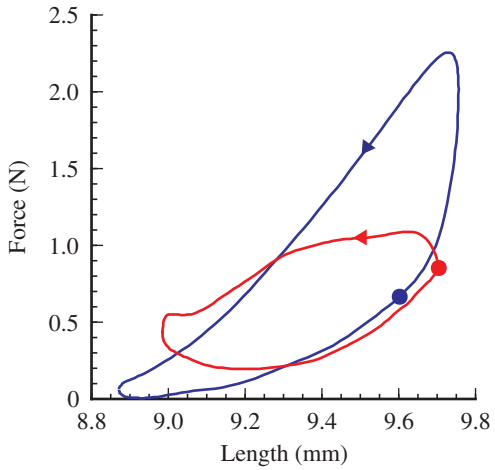

Fig. 6. Work loops measured under conditions that maximized power output [blue, phase of activation: 0.34; mean length: 9.81 mm (1.05L_{op}); peak-to-peak strain amplitude: 0.95L_{op}; power output: 91.0 W kg^{-1}] and under conditions that replicated conditions measured *in vivo* during tethered flight [red, phase of activation; 0.52, mean length: 9.81 mm (1.05L_{op}); peak-to-peak strain amplitude: 0.77L_{op}, power output: 53.9 W kg^{-1}]. Time progresses in each loop in a counterclockwise direction, as indicated by the arrowhead on each loop. The filled circle on each loop indicates the time of muscle activation. Both work loops are from Moth 1 in Tables 1 and 2. Activation of the muscle prior to the onset of shortening maximized power output. Under *in vivo* conditions in which muscle activated occurred near the onset of shortening, the muscle generated relatively low force during shortening and did not relax completely prior to lengthening.

Rheuben and Kammer, 1987; Wendler et al., 1993; Ando and Kanzaki, 2004). It is therefore unlikely that the *in vivo* performance of the dl_1 muscles reflects a compromise between power generation and direct control of wing kinematics. There remains, however, the possibility that submaximal power output by these muscles represents a design compromise related to some degree of intrinsic regulation of the wing stroke, maintenance of elevated thoracic temperature, efficiency, or coupling among different elements of the flight system.

The *in vivo* operating range of the dl_1 muscles lies entirely on the ascending limb of their isometric twitch length–tension curve (Tu and Daniel, 2004). Due to the steepness of this length–tension curve, transient increases in the wingstroke amplitude that increase in the strain of the dl_1 muscles will automatically enhance the capacity of these muscles to generate force. The combination of the length–tension characteristics of the dl_1 muscles, their pattern of activation, and their operating length range may therefore provide some degree of non-neuronal regulation of wingstroke frequency and amplitude. Such intrinsic regulation at the level of the muscle appears to come at the cost of power generation, since the *in vivo* operating length is substantially shorter than the operating length that maximizes power output.

As the largest muscles in the thorax of *Manduca*, the dl_1 muscles are likely to be the primary source of heat during pre-flight warm-up and during flight, in addition to their function as the primary wing depressors (Dotterweich, 1928). We do not know if submaximal power output by the dl_1 muscles is related to this dual role, or if the dl_1 muscles of non-endothermic moths generate power at levels approaching their maximum capacity. Interestingly, the red muscles of skipjack tuna also function to maintain regionally elevated muscle

Table 2. *Summary of the mechanical power output of the dl_1 measured under conditions of phase, mean length and strain amplitude that fell within the range of values measured* in vivo

Moth	Power (W kg^{-1})	% of max. power	Phase (fraction)	L_e	Strain amplitude	N
1	50.0±14.2	55.0	0.47±0.03	1.02±0.03	0.086±0.013	9
2	46.3±21.7	53.7	0.49±0.02	1.01±0.03	0.086±0.012	6
3	56.9±16.6	60.7	0.48±0.03	1.01±0.03	0.090±0.013	11
4	61.6±11.4	67.2	0.48±0.03	1.01±0.03	0.088±0.005	17
5	38.8±5.1	66.1	0.48±0.03	1.01±0.03	0.078±0.001	16
6	31.0±14.6	39.5	0.49±0.02	0.99±0.03	0.090±0.001	11
Mean	47.4±11.3	57.0	0.48±0.01	1.01±0.01	0.086±0.005	

Values are means ± 1 S.D.

Experimental length, L_e, is normalized to the operational length, L_{op}. N is the number of power measurements that matched the range of phase, mean length and strain amplitude that fell within the range of values measured *in vivo*.

temperatures (Barrett and Hester, 1964) while attaining maximal power output, suggesting that these two functions are not mutually exclusive.

We do not yet know the extent to which the efficiency of the dl_1 muscles may be optimized during flight. Maximum efficiency and maximum power output may not occur under the same conditions; Curtin and Woledge (1996) showed that the stimulus duty cycle that maximizes efficiency in dogfish swimming muscle differs from the duty cycle that maximizes power output. Although Josephson and Stevenson (1991) measured the efficiency of the dorsoventral muscles under conditions that optimize power output, the relationships between power, efficiency and operating parameters of the dl_1 muscles are unknown. A decrease in efficiency with increasing power output would suggest that submaximal power output during steady flight represents a compromise between optimization for power and muscle efficiency. Increased efficiency at higher levels of power output would be particularly puzzling since steady flight conditions would then be associated with both low power output and low efficiency.

In addition to potential compromises related to control, heat generation or efficiency, coupling between different elements of the flight system could constrain the temporal patterns of strain and activation in the dl_1 muscles to values that do not maximize power output. Controlled, stable locomotion arises from complex coupling between musculoskeletal mechanics, propulsors and the external medium, and neural control (Daniel, 1985; Daniel and Tu, 1999). The variables that determine muscle power output, especially length changes and the temporal pattern of activation, arise from interactions between these systems at multiple levels. The design of complex muscle systems could involve compromises that maximize the net power output at the level of the entire system rather than at the level of individual muscles. In addition, mechanical coupling between internal musculoskeletal mechanics and external fluid dynamics could impose constraints on the possible trajectories, amplitudes and frequencies of muscle length oscillations, and these constraints could conflict with maximum power output.

Finally, operation at submaximal levels of power output could leave reserves for use in extreme behaviors such as escape locomotion, instances where efficiency may be less critical. Our results suggest that flying *Manduca* could obtain most of this reserve power by advancing the phase at which they activate the dl_1 muscles. We do not yet know, however, if *Manduca* modulates the phase of activation of the dl_1 muscles during maneuvers. It is important to note that variation in aerodynamic power generation by the wings may not be directly coupled to variation in mechanical power generation by the dl_1 muscles. Transmission of mechanical power from the dl_1 muscles to the wings is potentially regulated by the actions of 12 pairs of flight muscles that insert directly onto elements of the wing articulation (Nüesch, 1953; Eaton, 1988). In flies, changes in the firing patterns of the small direct flight muscles can produce large changes in wing kinematics (Tu and Dickinson, 1996; Balint and Dickinson, 2001). These changes in wing kinematics are likely to occur independently of modulation of power output by the large elevator and depressor muscles, since in flies, these are asynchronous muscles that are not under direct neural control. Similar modulation in the phase and frequency of activation in direct flight muscles is seen in *Manduca* (Rheuben and Kammer, 1987; Kammer, 1971; Wendler et al., 1993; Ando and Kanzaki, 2004). Assesment of the range of possible modulation of power output in the dl1 muscles must await technologies that permit simultaneous measurement of muscle activation and muscle length changes in freely flying insects.

With the relatively small but growing number of muscles for which we can compare potential and realized power output, generalizations about muscle design may be premature. The available evidence does suggest, however, that maximal power output by muscles during locomotion may be restricted to burst performance and a small number of specialized cases such as thunniform swimmers. Understanding the principles that underlie the design of locomotor muscles will clearly require investigations into additional performance measures such as efficiency, as well as a better understanding of the consequences of coupling between neural control, musculoskeletal mechanics, and the external environment.

This work was supported by NSF Grant 9511681 to T.L.D., a Packard Interscience Grant to T.L.D., and by an ONR MURI Grant.

References

Ahn, A. N. and Full, R. J. (2002). A motor and a brake: two leg extensor muscles acting at the same joint manage energy differently in a running insect. *J. Exp. Biol.* **205**, 379-389.

Altringham, J. D., Wardle, C. S. and Smith, C. I. (1993). Myotomal muscle function at different locations in the body of a swimming fish. *J. Exp. Biol*. **182**, 191-206.

Ando, N. and Kanzaki, R. (2004). Changing motor patterns of the 3rd axillary muscle activities associated with longitudinal control in freely flying hawkmoths. *Zool. Sci*. **21**, 123-130.

Askew, G. N. and Marsh, R. L. (1997). The effects of length trajectory on the mechanical power output of mouse skeletal muscles. *J. Exp. Biol*. **200**, 3119-3131.

Askew, G. N. and Marsh, R. L. (2001). The mechanical power output of the pectoralis muscle of blue-breasted quail (*Coturnix chinensis*): the *in vivo* length cycle and its implications for muscle performance. *J. Exp. Biol.* **204**, 3587-3600.

Askew, G. N., Marsh, R. L. and Ellington, C. P. (2001). The mechanical power output of the flight muscles of blue-breasted quail (*Coturnix chinensis*) during take-off. *J. Exp. Biol.* **204**, 3601-3619.

Balint, C. N. and Dickinson, M. H. (2001). The correlation between wing kinematics and steering muscle activity in the blowfly *Calliphora vicina*. *J. Exp. Biol*. **204**, 4213-4226.

Barrett, I. and Hester, F. J. (1964). Body temperatures of yellowfin and skipjack tuna in relation to sea surface temperature. *Nature* **203**, 96-97.

Biewener, A. A., Konieczynski, D. D. and Baudinette, R. V. (1998). *In vivo* muscle force–length behavior during steady-speed hopping in tammar wallabies. *J. Exp. Biol.* **201**, 1681-1694.

Coughlin, D. J. (2000). Power production during steady swimming in largemouth bass and rainbow trout. *J. Exp. Biol.* **203**, 617-629.

Curtin, N. A. and Woledge, R. C. (1996). Power at the expense of efficiency in contraction of white muscle fibers from dogfish *Scyliorhinus canicula*. *J. Exp. Biol.* **199**, 593-601.

Daniel T. L. (1985). Invertebrate swimming: Integrating internal and external mechanics. In *Biological Fluid Dynamics* (ed. C. P. Ellington and T. J. Pedley), pp. 61-89. Cambridge: Society for Experimental Biology.

Daniel, T. L. and Tu, M. S. (1999). Animal movement, mechanical tuning and coupled systems. *J. Exp. Biol.* **202**, 3415-3421.
Dotterweich, H. (1928). Beitrgäge zur Nervenphysiologie der Insekten. *Zool. Jb. Abt. Allg. Zool. Physiol. Tiere*. **44**, 399-450.
Eaton, J. L. (1988). *Lepidoptean Anatomy*. New York: Wiley Interscience.
Franklin, C. E. and Johnston, I. A. (1997). Muscle power output during escape responses in an Antarctic fish. *J. Exp. Biol.* **200**, 703-712.
Full, R. J., Stokes, D. R., Ahn, A. N. and Josephson, R. K. (1998). Energy absorption during running by leg muscles in a cockroach. *J. Exp. Biol.* **201**, 997-1012.
Gilmour, K. M. and Ellington, C. P. (1993). *In vivo* muscle length changes in bumblebees and the *in vitro* effects on work and power. *J. Exp. Biol.* **183**, 101-113.
Girgenrath, M. and Marsh, R. L. (1999). Power output of sound-producing muscles in the tree frogs *Hyla ersicolor* and *Hyla chrysoscelis*. *J. Exp. Biol.* **202**, 3225-3237.
Hammond, L., Altringham, J. D. and Wardle, C. S. (1998). Myotomal slow muscle function of rainbow trout *Onchorynchus mykiss* during steady swimming. *J. Exp. Biol.* **201**, 1659-1671.
Hedrick, T. L., Tobalske, B. W. and Biewener, A. A. (2003). How cockatiels (*Nymphicus hollandicus*) modulate pectoralis power output across flight speeds. *J. Exp. Biol.* **206**, 1363-1378.
Heinrich, B. (1971). Temperature regulation of the sphinx moth, *Manduca sexta* I. Flight energetics and body temperature during free and tethered flight *J. Exp. Biol.* **54**, 141-152.
Heinrich, B. and Bartholomew, G. A. (1971). An analysis of pre-flight warm-up in the sphinx moth *Manduca sexta*. *J. Exp. Biol.* **55**, 223-239.
Hill, A. V. (1950). The dimensions of animals and their muscular dynamics. *Sci. Prog*. **38**, 209-230.
James, R. S. and Johnston, I. A. (1998). Scaling of muscle performance during escape responses in the fish *Myxocephalus scorpius* L. *J. Exp. Biol.* **201**, 913-923.
Josephson, R. K. (1985a). Mechanical power output from striated muscle during cyclic contraction. *J. Exp. Biol.* **114**, 493-512.
Josephson, R. K. (1985b). The mechanical power output of a tettigoniid wing muscle during singing and flight. *J. Exp. Biol.* **117**, 357-368.
Josephson, R. K. (1989). Power output from skeletal muscle during linear and sinusoidal shortening. *J. Exp. Biol.* **147**, 533-537.
Josephson, R. K. (1997). Power output from a flight muscle of the bumblebee *Bombus terrestris* II. Characterization of the parameters affecting power outuput. *J. Exp. Biol.* **200**, 1227-1239.
Josephson, R. K. and Ellington, C. P. (1997). Power output from a flight muscle of the bumblebee *Bombus terrestris*. I. Some features of the dorso-ventral flight muscle. *J. Exp. Biol.* **200**, 1215-1226.
Josephson, R. K. and Stevenson, R. D. (1991). The efficiency of a flight muscle from the locust *Schistocerca americana*. *J. Physiol.* **442**, 413-429.
Josephson, R. K., Malamud, J. G. and Stokes, D. R. (2000). Asynchronous muscle: a primer. *J. Exp. Biol.* **203**, 2713-2722.
Kammer, A. E. (1967). Muscle activity during flight in some large Lepidoptera. *J. Exp. Biol.* **47**, 277-295.
Kammer, A. E. (1971). The motor output during turning flight in a hawkmoth, *Manduca sexta*. *J. Insect Physiol.* **17**, 1073-1086.
Lutz, G. J. and Rome, L. C. (1996). Muscle function during jumping in frogs. I. Sarcomere length changes, EMG pattern, and jumping performance. *Am. J. Physiol.* **271**, C563-C670.
Machin, K. E. and Pringle, J. W. S. (1960). the physiology of insect fibrillar muscle II. The effect of sinusoidal changes of length on a beetle flight muscle. *Proc. R. Soc. Lond. B* **152**, 311-330.
Marden, J. H., Fitzhugh, G. H., Girgenrath, M., Wolf, M. R. and Girgenrath, S. (2001). Alternative splicing, muscle contraction and intraspecific variation: associations between troponin T transcripts, Ca^{2+} sensitivity and the force and power output of dragonfly flight muscles during oscillatory contraction. *J. Exp. Biol.* **204**, 3457-3470.
Marsh, R. L. and Olson, J. M. (1994). Power output of scallop adductor muscle during contractions replicating the *in vivo* mechanical cycle. *J. Exp. Biol.* **193**, 139-156.
Marsh, R. L., Olson, J. M. and Guzik, S. K. (1992). Mechanical performance of scallop adductor muscle during swimming. *Nature* **357**, 411-413.
McCrea, M. J. and Heath, J. E. (1971). Dependence of flight on temperature regulation in the moth, *Manduca sexta*. *J. Exp. Biol.* **54**, 415-435.
Mizisin, A. P. and Josephson, R. K. (1987). Mechanical power output of locust flight muscle. *J. Comp. Physiol. A* **160**, 413-419.
Nüesch, H. (1953). The morphology of the thorax of *Telea Polyphemus* (Lepidoptera). I. Skeleton and muscles. *J. Morph. Phil.* **93**, 589-608.
Olson, J. M. and Marsh, R. L. (1998). Activation patterns and length changes in hindlimb muscles of the bullfrog *Rana catesbeiana* during jumping. *J. Exp. Biol.* **201**, 2763-2777.
Rheuben, M. B. and Kammer, A. E. (1987). Structure and innervation of the third axillary muscle of *Manduca* relative to its role in turning flight. *J. Exp. Biol*. **131**, 373-402.
Roberts, J. R., Marsh, R. L., Weyland, P. G. and Taylor, C. R. (1997). Muscular force in running turkeys: The economy of minimizing work. *Science* **275**, 1113-1115.
Rome, L. C., Swank, D. M. and Coughlin, D. J. (1999). The influence of temperature on power production during swimming. II. Mechanics of red muscle fibers *in vivo*. *J. Exp. Biol.* **202**, 333-345.
Stevenson, R. D. and Josephson, R. K. (1990). Effects of operating frequency and temperature on mechanical power output from moth flight muscle. *J. Exp. Biol.* **149**, 61-78.
Swank, D. M. and Rome, L. C. (2001). The influence of thermal acclimation on power production during swimming. II. Mechanics of scup red muscle under *in vivo* conditions. *J. Exp. Biol.* **204**, 419-430.
Syme, D. and Shadwick, R. E. (2002). Effects of longitudinal body position and swimming speed on mechanical power of deep red muscle from skipjack tuna (*Katsuonus pelamis*). *J. Exp. Biol.* **205**, 189-200.
Tu, M. S. and Dickinson, M. H. (1994). Modulation of negative work output from a steering muscle of the blowfly *Calliphora vicina*. *J. Exp. Biol.* **192**, 207-224.
Tu, M. S. and Daniel, T. L. (2004). Cardiac-like behavior of an insect flight muscle. *J. Exp. Biol.* **207**, 2455-2464.
Tublitz, N. J. and Truman, J. W. (1985). Insect cardioactive peptides. I. Distribution and molecular characteristics of two cardioacceleratory peptides in the tabacco hawkmoth *Manduca sexta*. *J. Exp. Biol.* **114**, 365-379.
Wendler, G. Muller, M. and Dombrowski, U. (1993). The activity of pleurodorsal muscles during flight and at rest in the moth *Manduca sexta* (L.). *J. Comp. Physiol.* **173**, 65-75.
Willmott, P. A. and Ellington, C. P. (1997). The mechanics of flight in the hawkmoth *Manduca sexta*. I. Kinematics of hovering and forward flight. *J. Exp. Biol*. **200**, 2705-2722.